Leadership in Sustainable Infrastructure

Leadership en Infrastructures Durables

Vancouver, Canada

May 31 – June 3, 2017/ *Mai 31 – Juin 3, 2017*

NUMERICAL MODELING OF REINFORCED ECC BUILDING FRAMES

Melnikov R.[1,4], Hossain K. M. A.[2]
[1] Master's of Engineering Student, Ryerson University, Canada
[2] Professor of Civil Engineering, Ryerson University, Canada
[4] roman.melnikov@ryerson.ca

Abstract: This paper is focused on the numerical modeling of reinforced concrete frame incorporating high performance concretes: self-consolidating concrete (SCC) and engineered cementitious composite (ECC). The numerical modeling of one-story SCC and ECC frames were conducted using finite element (FE) software ABAQUS Implicit. The developed three dimensional beam-column finite element model (FEM) was subjected to displacement controlled monotonic lateral loading until failure. The material properties were obtained from previous and current experimental research studies. The FE model frame performance was evaluated based on load capacity, ductility, mode of failure and crack patterns compared to those of obtained from experimental studies. Also, ECC/SCC frames with two different reinforcement configurations (flexure controlled and shear controlled) were modeled and analyzed. The study revealed superior ductility and load carrying capacity of ECC frame. Furthermore, the ECC frames showed more uniform crack distribution at the critical regions, compared to those with SCC. FE parametric simulations showed that the use of ECC material with larger tensile strain capacity resulted in the development of more uniform stress in reinforcement in the frame critical regions.

1 INTRODUCTION

Present and future infrastructure needs dictate ongoing innovation and improvement of existing construction methods and materials. As such, effective and durable materials have been and are being developed including self-consolidating concrete (SCC) and strain hardening cementitious composite (also called Engineered Cementitious Composite 'ECC'). Main driver behind developing these materials is to prolong life of the infrastructure and minimize construction and maintenance costs.

SCC was developed to overcome the issue of construction defects due to limited skilled labor available in Japan at the time (Okamura 1997). SCC flows under its own weight with no need for external vibration. It is an ideal material to use in areas of dense reinforcement or irregularly shaped areas. SCC usage results in better quality structures, reduced labor and no inconvenience associated with vibration when compared to regular concrete. The higher fluidity of SCC is achieved by using larger proportion of fine aggregate (typically more than 50%) and superplasticizers. Mineral fillers such as fly ash are typically added to improve workability.

ECC was developed with the goal to eliminate or postpone crack localization and increase tensile strain capacity of concrete. This goal is achieved through micromechanics principles used in design of the material, namely (Wang and Li 2004). Based on the strength principle, the matrix cracking strength must

be lower than the bridging strength of the fiber. While the energy principle ensures stable (or flat) cracks when the strain energy released at the crack tip is absorbed by the bridging fibers and, thus, does not exceed the energy required to grow the crack surfaces. Combination of strength and energy principles during material development results in multiple fine cracking, and ECC achieving superior tensile straining prior to crack localization and failure at up to 5% elongation (Li 2003). The high strain capacity and multi-cracking properties make ECC an ideal durable material for construction. Given the worldwide demand for infrastructure systems, the potential application of ECC either in new construction or as repair material is enormous. The use of reinforced ECC in construction is an emerging technology and can lead to structural systems with enhanced ductility, durability, energy absorbing capacity and service life compared with traditional systems.

This paper presents the finite element modeling (FEM) of reinforced one story flexure and shear critical beam-column frames made of SCC and ECC based on experimental results. The performance of FE models was judged based on load-deflection response, strain development, cracking and failure modes.

2 EXPERIMENTAL BACKGROUND

Research has been conducted at Ryerson University (Yeganeh 2013) to study the structural performance of one-story frames (approximately 1/3 the size of typical building frame) made of SCC and ECC. The frames were subjected to monotonic lateral loading to failure. Two types of reinforcement configurations were used, namely: flexure-critical and shear-critical, difference being removal of stirrups in the shear-critical frame. To induce “weak beam-strong column concept”, the beam was provided with 10 mm longitudinal reinforcement with 15 mm clear cover and the column was provided with 15 mm longitudinal reinforcement with 10mm clear cover.

ECC was made of high proportion of fly ash (1.2 parts per 1 part of cement), natural grain silica sand (nominal size of 110µm) and Poly vinyl alcohol (PVA) fibers (with nominal length of 8 mm and diameter of 39µm). Ultimate tensile strength of PVA fibers was 1620 MPa and modulus of elasticity was 42.8GPa. Water-cement ratio of the ECC mix was 0.27 and polycarboxylate high range water reducer was added to the mix. SCC was made with commercially available dry content pre-packaged bags. SCC included silica fume, air-entraining admixture and 10 mm maximum size coarse aggregate.

All frames were cast separately cured until testing at 28 days. During testing, the frames were connected to a base beam which was rigidly connected to the strong floor. To enhance the fixity of supports, steel plates were inserted into clearances between the columns and base beam during the experiment.

Compression (ASTM C39-03) and four-point bending tests (ASTM C78-10) were performed on SCC and ECC control specimens after 28 days of curing. Direct tensile testing was performed on steel coupons collected representing beam, steel and stirrup rebars (Yeganeh 2013).

The experimental study revealed that the ECC frame showed greater load capacity and ductility in terms of displacement compared to SCC frame having both flexure and shear critical reinforcement configurations (refer to Table 1).

Table 1: Experimental Results Summary (Yeganeh 2013)

Material and Frame Type	Ultimate load (kN)	Ultimate Displacement (mm)
SCC-flexure critical	59.5	65.19
ECC-flexure critical	77.5	82.66
SCC-shear critical	29.5	29.24
ECC-shear critical	56.46	51.60

SCC and ECC flexural frames failed in combined flexure-shear mode, forming a large crack that initiated at the beam tension face near column and propagated to the beam’s compression face. ECC frame had also shown multiple cracking in critical regions as opposed to SCC frame.

SCC shear critical frame failed in shear mode near the column base. In comparison, the failure mode of ECC shear critical frame was the same as flexure critical ECC frame (flexure-shear failure in the beam region near the column). The shear critical ECC frame showed multiple hairline cracking in the column region but did not fail at that location.

3 NUMERICAL MODELING

3.1 Material Parameters

Numerical modeling of SCC and ECC frames were conducted using FEM software ABAQUS Implicit. Isotropic elastic-plastic model was used for steel with stress-strain data (Table 2) obtained from uniaxial tests conducted on steel coupons (Yeganeh 2013). The uniaxial stress-strain data was converted to true stress – true strain data prior to input in FE model.

Table 2: Steel Material Parameters Used for Simulation

	Yield Stress (MPa)	Yield Strain	Ultimate Stress (MPa)*	Ultimate Strain
Beam Longitudinal Bars (10mm)	527	0.002240	577	0.01
Column Longitudinal Bars (15mm)	478	0.002310	528	0.01
Beam and Column Transverse Bars (6mm)	429	0.002	479	0.01

*Strain hardening was introduced to avoid convergence issues in simulation

Concrete Damaged Plasticity (CDP) material model was used for ECC and SCC. It is based on concepts of isotropic elastoplasticity combined with material damage (Dassault Systemes 2009). CDP model allows for material hardening and uses non-associated plastic flow rule. To simplify numerical algorithm, elastoplastic constitutive relations are decoupled from damage response (Lee and Fenves 1998). CDP parameters were selected as follows: dilatation angle (ψ) = 15°; eccentricity of the plastic potential (ϵ) = 0.1 (software default); $\frac{\sigma_{b0}}{\sigma_{c0}}$ (ratio of biaxial compressive strength to uniaxial compressive strength) = 1.16 (software default); $K_c = \frac{\bar{q}_{TM}}{\bar{q}_{CM}}$ (ratio of Mises equivalent effective stress at tensile meridian to the same stress at compressive meridian in principal effective stress space) = 0.667 (software default); viscoplastic regularization parameter (μ) = 0.00001. The angle of dilatation was selected as 15° based on previous studies recommendations (Szczecina et al. 2016, Vermeer et al. 1984). Viscoplastic regularization was introduced to overcome convergence difficulty, and a small value was selected to minimize rate dependency. Table 3 summarizes concrete material parameters used in simulation: parameters that were not obtained by direct testing (e.g. tensile strain capacity of ECC) were estimated by using existing experimental data and empirical relations.

Table 3: Concrete Material Parameters Used in FE Modeling

Parameters	SCC	ECC
f'_c (maximum compressive stress)	50.6MPa; obtained from experiment (Yeganeh 2013)	63.5MPa; obtained from experiment (Yeganeh 2013)
ε'_c compressive strain at maximum stress)	0.0023; Popovics model for uniaxial compression (Popovics 1970): [1] $\varepsilon'_c = \frac{f'_c}{E_c}(\frac{n}{n-1})$, where: f'_c – compressive strength, E_c – Young's modulus of concrete, $n = 0.8 + \frac{f'_c}{17}$ is a curve fitting factor	0.0043; Popovics model for uniaxial compression (Popovics 1970): [1] $\varepsilon'_c = \frac{f'_c}{E_c}(\frac{n}{n-1})$, where: f'_c – compressive strength, E_c – Young's modulus of concrete, $n = 0.8 + \frac{f'_c}{17}$ is a curve fitting factor

Compressive stress-strain relationship	Popovics model for uniaxial compression (Popovics 1970): [2] $f = \frac{n(f'_c)(\frac{\varepsilon}{\varepsilon'_c})}{n-1+(\frac{\varepsilon}{\varepsilon'_c})^{nk}}$, where: f'_c – compressive strength, ε – compressive variable strain, ε'_c – compressive strain corresponding to f'_c, $n = 0.8 + \frac{f'_c}{17}$ is a curve fitting factor, $k = 1$ for $\frac{\varepsilon_c}{\varepsilon'_c} \leq 1$ and $k = 0.67 + \frac{f'_c}{62}$ for $\frac{\varepsilon_c}{\varepsilon'_c} > 1$ is decay factor	Popovics model for uniaxial compression (Popovics 1970): [2] $f = \frac{n(f'_c)(\frac{\varepsilon}{\varepsilon'_c})}{n-1+(\frac{\varepsilon}{\varepsilon'_c})^{nk}}$, where: f'_c – compressive strength, ε – compressive variable strain, ε'_c – compressive strain corresponding to f'_c, $n = 0.8 + \frac{f'_c}{17}$ is a curve fitting factor, $k = 1$ for $\frac{\varepsilon_c}{\varepsilon'_c} \leq 1$ and $k = 0.67 + \frac{f'_c}{62}$ for $\frac{\varepsilon_c}{\varepsilon'_c} > 1$ is decay factor
Compressive damage evolution	d_c was assumed to gradually increase from 0 (at onset of plastic strain) to 0.99*	d_c was assumed to gradually increase from 0 (at onset of plastic strain) to 0.99*
f_t (maximum tensile stress)	2.95MPa; ACI 318-08 code, section 22.5 equation for plain concrete ([3] $f_t = 5\sqrt{f'_c}$ (psi)) (ACI 2008)	2.50MPa; estimated from SHCC empirical curve of Tensile Strain Capacity versus ratio of Modulus of Rupture (MOR)/Tensile Strength, obtained by (Qian and Li 2008) where: MOR – Modulus of Rupture obtained from ECC four-point-bending test (Yeganeh 2013), tensile strain capacity obtained from ε-δ master curve by (Qian and Li 2007)**
ε'_t (tensile strain at maximum stress)	0.000097; obtained from linear relationship $\varepsilon'_t = \frac{E_t}{f_t}$	0.003; estimated from ECC master curve (Qian and Li 2007) based on experimental four-point bending curves for SHCC: [4] $\varepsilon'_t = 0.50\delta_u - 0.22$, where: δ_u – tensile deflection capacity obtained from FPBT (Yeganeh 2013)**
Tensile stress-strain relationship	linear up to f_t; tension stiffening model for softening part (modified from Vecchio et al. 1986), [5] $f = \frac{f_t}{1+\sqrt{500\varepsilon}}$, where: f_t – tensile strength, ε – tensile variable strain	linear up to f_{cr} (cracking strength, assumed as 2.4MPa); linear hardening to f_t; tension stiffening model for softening part (modified from Vecchio et al. 1986), [5] $f = \frac{f_t}{1+\sqrt{500\varepsilon}}$, where: f_t – tensile strength, ε – tensile variable strain
Tensile damage evolution	d_t was assumed to gradually increase from 0 (at onset of plastic strain) to 0.99*	d_t was assumed to gradually increase from 0 (at onset of plastic strain) to 0.99*
E (Young's modulus)***	30374MPa; CSA A23.3 code equation [6] $E_c = 3300\sqrt{f'_c} + 6900)\left(\frac{\gamma_c}{2300}\right)^{1.5}$ where: γ_c – density of concrete (Cement Association of Canada 2006), f'_c – compressive strength	19034MPa; JSCE Recommendations for Design of HPFRCC (Section 3.4) equation [7] $E_c = 1.77 * 10^4 * \sqrt{\frac{\gamma_\omega}{18.5}}(\sqrt[3]{\frac{f'_c}{60}})$ where: γ_ω – unit weight of concrete (JSCE 2008), f'_c – compressive strength
γ_c (density)	2300kg/m^3; Material data provided by manufacturer (Yeganeh 2013)	2100kg/m^3; assumed

μ (Poisson's ratio)	0.2; assumed	0.23; JSCE recommendations for Design of HPFRCC (Section 3.5) (JSCE 2008)

*Damage evolution data was assumed for SCC and ECC materials. Stiffness degradation parameters (d_t and d_c) were assumed to gradually increase from 0 to 0.99 with increase of plastic strain.
**Direct tensile strength and tensile strain capacity for ECC was estimated from experimental four-point bending test (FPBT) results by using the inverse method proposed by (Qian and Li 2007). Master curve relating deflection obtained from FPBT and tensile strain capacity for 20 tested SHCC beams by (Qian and Li 2007) was used to estimate ECC's tensile strain capacity (equation [4] in Table 3). Maximum tensile strength of ECC was estimated by using SHCC master curve relating tensile strain capacity and ratio of MOR/tensile strength provided by (Qian and Li 2008).
***Young's modulus was assumed the same in tension and compression

3.2 FE Model Overview

The frame was modeled in ABAQUS, mimicking the structural dimensions and detailing from the experiment (Yeganeh 2013). Semi-rigid frame supports were simulated by means of fixed analytical rigid surfaces and pins to reduce computational costs. Contact interactions between concrete and steel surfaces were defined with Coulomb friction model and penalty constraint enforcement for pressure-overclosure behavior.

Concrete was modeled using linear continuum elements with reduced integration, and reinforcement was modeled using linear truss elements. Mesh size for the structure was selected as 40 mm from extensive mesh optimization simulations. Concrete-steel bond was enforced by means of element embedment constraint. Lateral displacement was applied over a surface via coupled node by using distributing coupling constraint. Self-weight of the structure was considered by applying gravity loading, and non-linear geometry effects were not considered.

3.3 FE Simulation and Comparison with Experimental Results

Load-lateral displacement data was collected from the FE simulations and compared against corresponding experimental data. Load-displacement responses, load capacity, strain development and failure modes obtained from FEM and experiments for flexure and shear critical frames are presented and compared in the following sections.

3.3.1 Flexure Critical Frames

Similar to experiments, FE simulation showed ECC frame to be more ductile than SCC frame (showing 62.84 mm versus 40.49mm ultimate displacement) and to have more load capacity than SCC frame (67.7kN versus 52.7kN) (Figures 1 and 2; Table 4). FE models underestimated maximum load capacity and ultimate displacement of both ECC (about 12.7% and 24%, respectively) SCC (11.5% and 38%, respectively) frames compared to experiments. The discrepancy in SCC frame simulation can be attributed to modeling technique (i.e. dowel action was not accounted for), underestimated tension stiffening effect and damage evolution law that assumed maximum stiffness degradation in tension and compression (i.e. 99%). The discrepancy in ECC frame simulation can be attributed to the possible underestimation of tensile strength and strain capacity as well as the damage evolution law that assumed maximum stiffness degradation. In both cases beam steel yielding was found to be the primary failure mode (as observed in experiments) with ECC frame yielding at 35.88 mm displacement and SCC frame yielding at 21.71m displacement (Figures 1 and 2). Similar to experiments, FE models showed stress concentration (red coloured squares) near the beam-column joints for both ECC and SCC frames (Figure 3). Based on the plots of maximum principal strain (Figure 3), it is observed that ECC frame showed less localized straining compared to its SCC counterpart at the same displacement, and conclusion of more uniform cracking pattern for ECC frame can be made. In general, FE models seemed to reasonably predict (about 12% difference) the ultimate load capacity of the ECC/SCC flexural critical frames.

Figure 1: Load-Displacement Curves for Flexure Critical ECC Frame

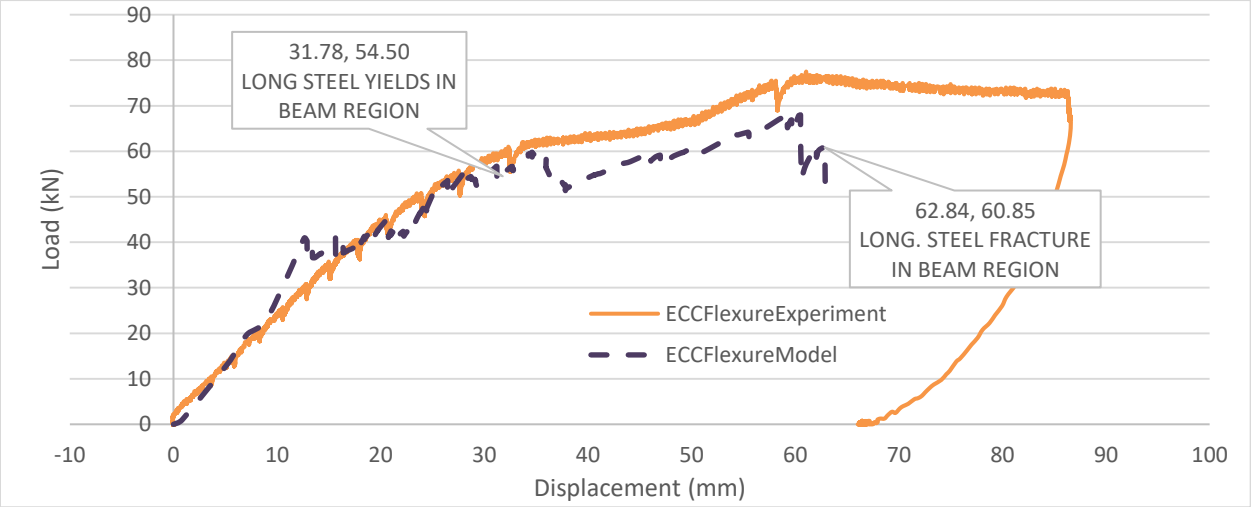

Figure 2: Load-Displacement Curves for Flexure Critical SCC Frame

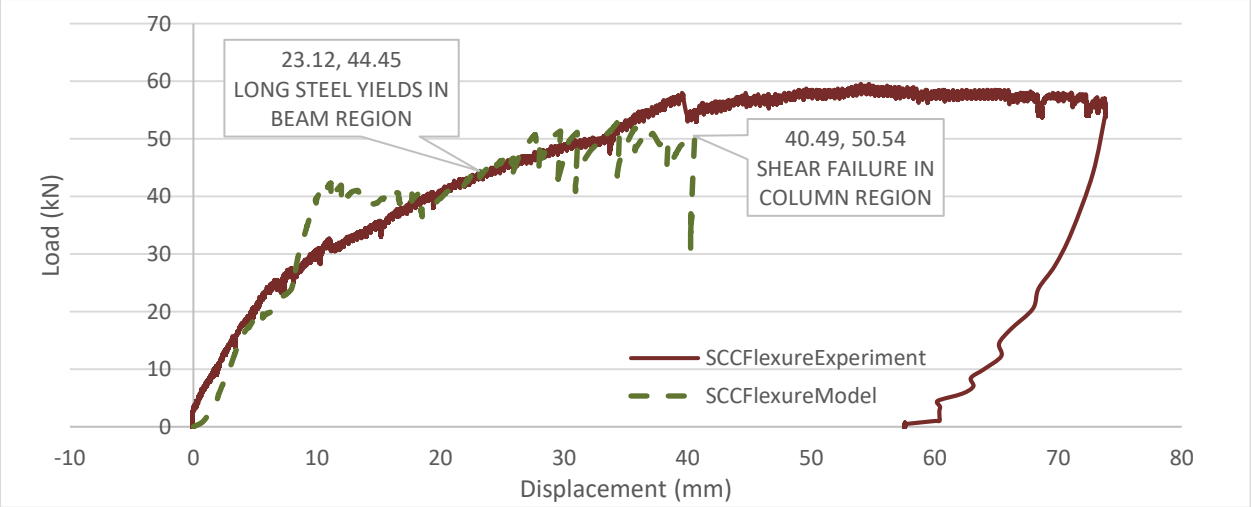

Table 4: Simulation and Experimental Results Comparison

	ECC Flexure Critical	SCC Flexure Critical	ECC Shear Critical	SCC Shear Critical
Load Capacity (kN, FE simulation)	67.70	52.70	63.07	48.00
Load Capacity (kN, experiment)	77.50	59.50	56.46	29.50
Difference (%)	12.65	11.42	10.48	38.54
Ultimate Deflection (mm, FE simulation)	62.84	40.49	43.72	29.95
Ultimate Deflection (mm, experiment)	82.66	65.19	51.60	29.24
Difference (%)	23.98	37.89	15.27	2.43

Figure 3: Maximum Principal Strains of Flexure Critical Frames (at 20mm lateral displacement): a) SCC, b) ECC

a) b)

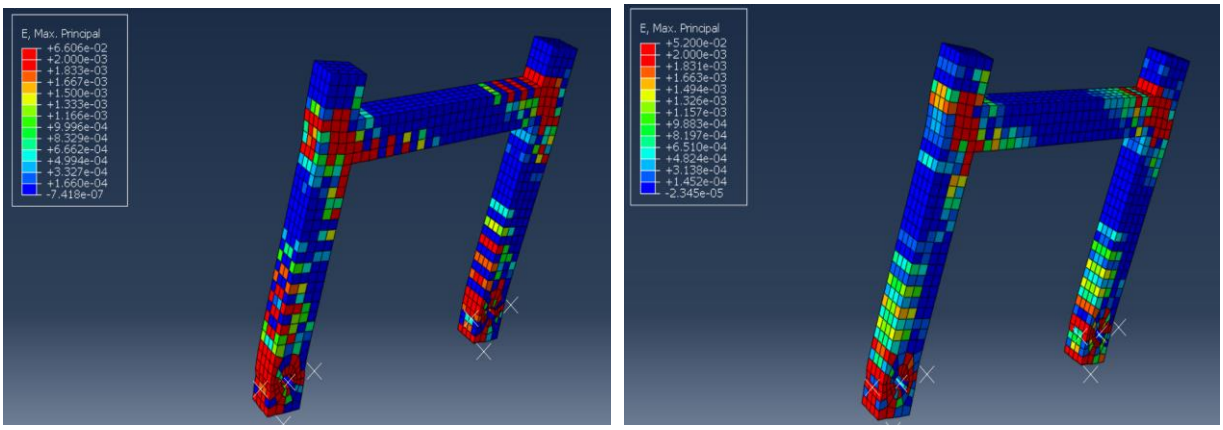

3.3.2 Shear Critical Frames

Figures 4 and 5 compare FE load-displacement responses of ECC and SCC shear critical frames with those obtained from experiments. Both FEM and experiments showed that the ECC frame was more ductile (exhibited higher displacement) and had greater load capacity compared to SCC frame (Table 4, Figures 4 and 5). It must be noted that the ECC frame failed due to beam steel yielding at 33.96 mm displacement showing flexure model of failure (as observed in experiment). On the other hand, similar to experiments SCC frame failed in shear mode of failure and no steel yielding was observed.

Figure 4: Load-Displacement Curves for Shear Critical ECC Frames

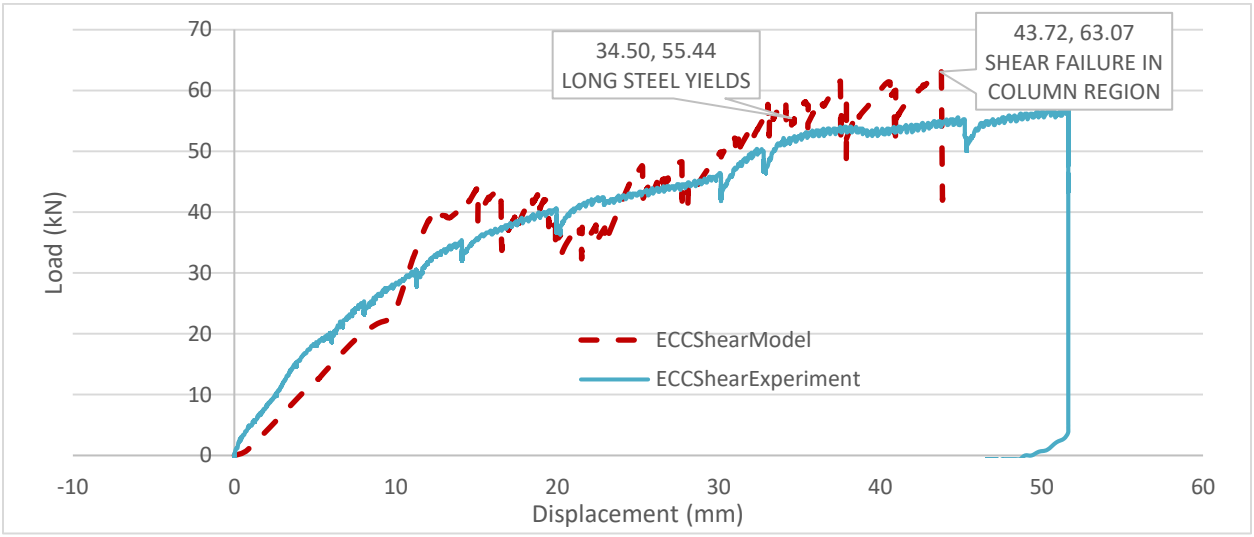

Figure 5: Load-Displacement Curves for Shear Critical SCC Frames

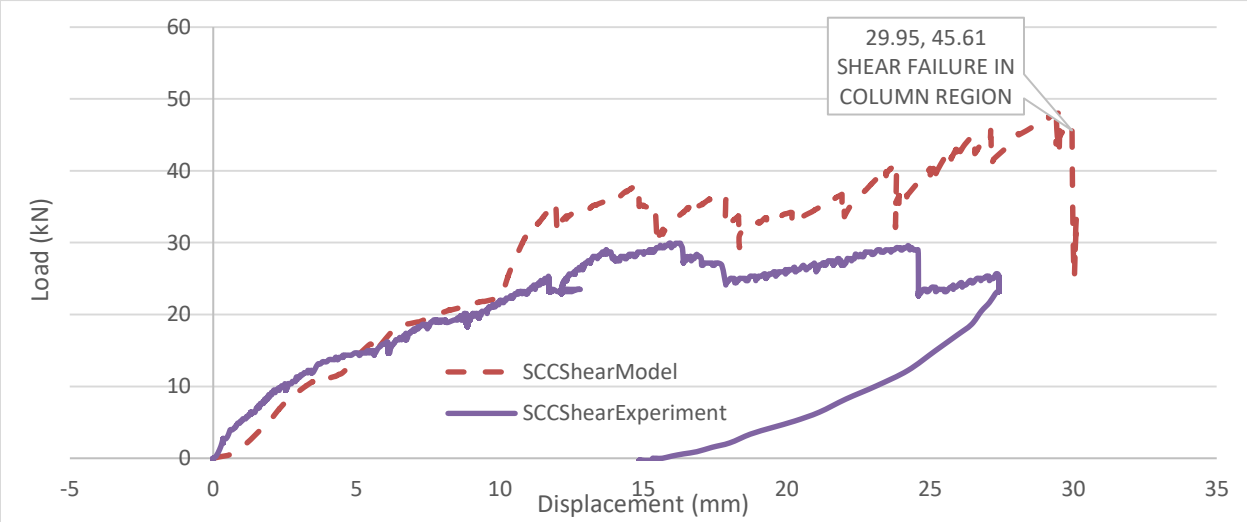

3.4 Parametric Study on ECC Frame

Parametric study was conducted to evaluate the effect of higher tensile strain capacity of ECC on the strain development in the reinforcement. ECC strain capacity was increased from 0.30% to 0.70% keeping all other parameters and model geometry the same. Flexure critical models were used for parametric analyses. Based on load-displacement responses (Figure 6), it is observed that increasing tensile strain capacity of ECC resulted in frame with increased ductility, but lower strength. Steel strain development was evaluated in four model elements: two elements in beam critical regions (designated as 1 and 2) and two elements in column critical regions (designated as 3 and 4) as shown in Figure 7. Longitudinal steel had not yielded in the frame with 0.70% ECC tensile capacity in beam and column regions (Figure 8). The frame with 0.70% ECC ultimately failed in shear (as indicated in Figure 6). It is expected that increasing tensile strength of ECC would result in increased load capacity and preferred mode of failure (longitudinal beam steel yielding) while maintaining the ductility of the frame at its highest.

Figure 6: Load-Displacement Curves for ECC Parametric Analysis

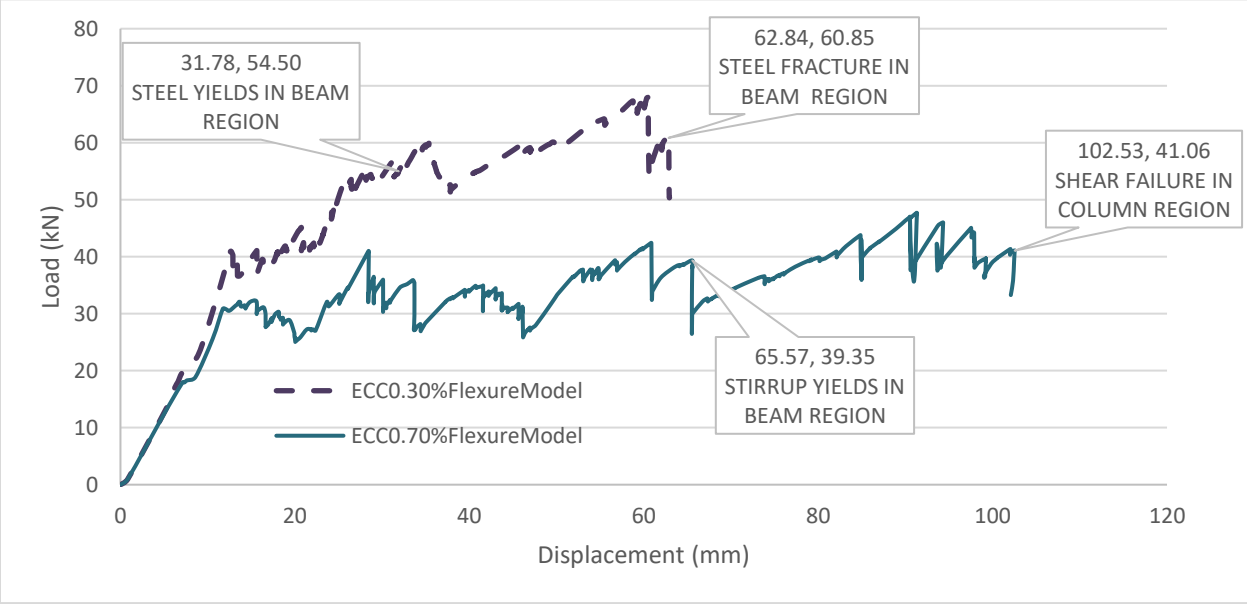

Figure 7: Steel Elements Used for Strain Comparison

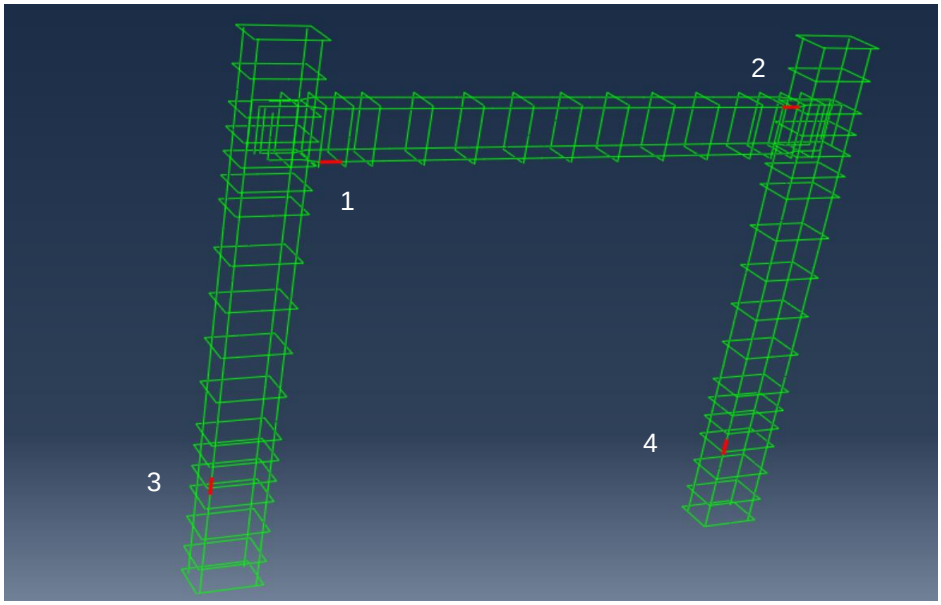

Figure 8: Comparative Strain Development in ECC Parametric Analysis: a) element 1 (beam), b) element 2 (beam), c) element 3 (column), d) element 4 (column)

a)

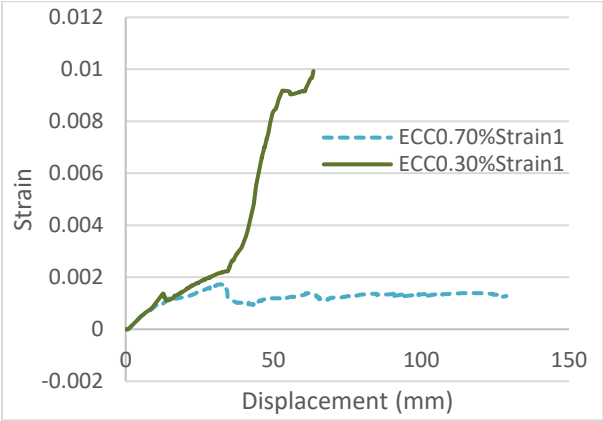

b)

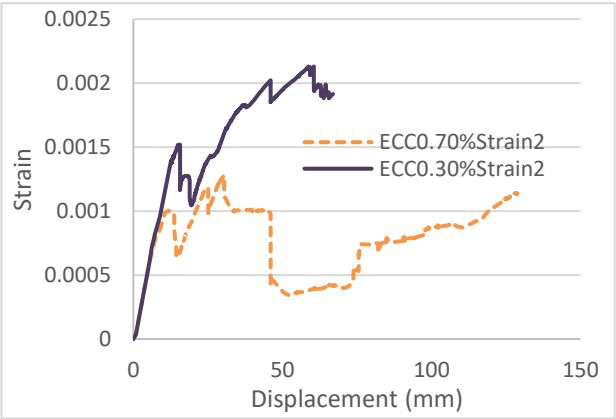

c)

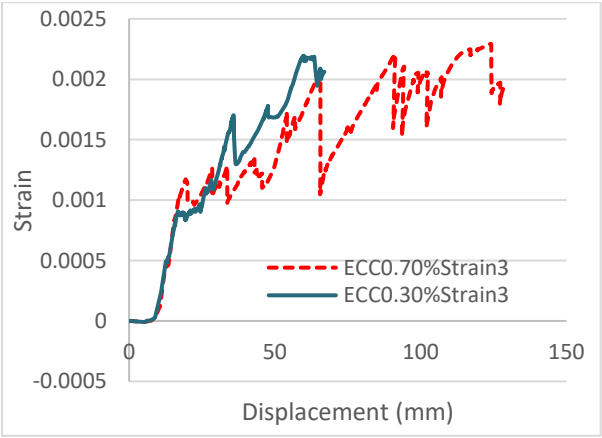

d)

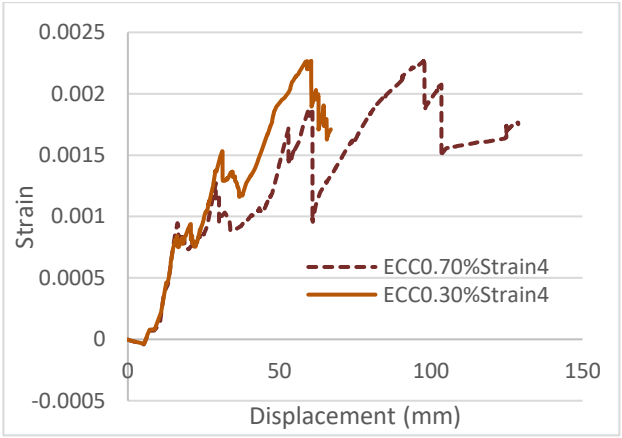

4 CONCLUSIONS

This study aimed at developing finite element models (FEMs) for simulating load-displacement response, steel strain development and failure modes of reinforced flexure and shear critical one story beam-column frame made of engineered cementitious composite (ECC) and self-consolidating concrete (SCC). The performance of FEMs was validated with experimental results. FEM were found to reasonably predict the load capacity (maximum 13% difference) of ECC shear and flexure critical frames. While FEM reasonably simulated the load capacity of SCC flexure critical frame (with about 11% difference), it could not simulate the load capacity of SCC shear critical frame (39% difference). FEMs under predicted the displacement capacity of ECC and SCC frames although seemed to simulate the displacement capacity of SCC shear critical frame. FEMs simulated failure modes, critical regions of failure and steel strain development of both ECC and SCC frames reasonably well. FE models were also able to simulate the high ductility characteristics and strain hardening capacity of ECC frames compared to their SCC counterparts. It was also shown from parametric FE simulations that the incorporation of ECC with higher tensile strain capacity would result in delayed yielding of reinforcing steel and lead to greater ductility. Further study is needed to fine tune the developed FE models using more experimental results and through refining the ECC material properties such as damage evolution law, concrete yield surface and plastic dilatation parameters.

REFERENCES

American Concrete Institute. 2008. *Building code requirements for structural concrete (ACI 318-08) and commentary*. Farmington Hills, MI, USA.

Collins, M., Mitchell, D., MacGregor J. 1993. Structural Design Considerations for High-Strength Concrete. *Concrete International*, **15**(5): 27-34.

Cement Association of Canada, 2006. *Concrete design handbook*, Cement Association of Canada, Ottawa, Canada.

Dassault Systemes. 2009. *ABAQUS Analysis User's Manual*, Version 6.9

Jankowiak, T., Lodygowski, T. 2005. Identification of Parameters of Concrete Damage Plasticity Constitutive Model. *Foundations of Civil and Environmental Engineering*, (6): 53-69.

Japan Society of Civil Engineers. 2008. *Recommendations for Design and Construction of High Performance Fiber Reinforced Cement Composites with Multiple Fine Cracks*, Concrete Committee, JSCE, Japan.

Kmiecik, P., Kamiński M. 2011. Modelling of reinforced concrete structures and composite structures with concrete strength degradation taken into consideration, *Archives of Civil and Mechanical Engineering,* **11**(3): 623-36.

Lee, J., Fenves, G. 1998. A plastic-damage concrete model for earthquake analysis of dams. *Earthquake Engineering & Structural Dynamics,* **27**(9): 937-56.

Li, V. 2003. On Engineered Cementitious Composites (ECC), *Journal of Advanced Concrete Technology* **1**(3): 215-30.

Okamura, H. 1997. Self Compacting High Performance Concrete – Ferguson Lecture for 1996, *Concrete International*, **19**(7): 50 – 54.

Qian, S., Li V. 2007. Simplified Inverse Method for Determining the Tensile Strain Capacity of Strain Hardening Cementitious Composites, *Journal of Advanced Concrete Technology* **5**(2): 235-46.

Qian, S., Li V. 2008. Simplified Inverse Method for Determining the Tensile Properties of Strain Hardening Cementitious Composites (SHCC), *Journal of Advanced Concrete Technology* **6**(2): 353-63.

Szczecina, M., Winnicki, A. 2016. Selected Aspects of Computer Modeling of Reinforced Concrete Structures. *Archives of Civil Engineering* **62**(1).

Vecchio, F., Collins, M. 1986. The Modified Compression-Field Theory for Reinforced Concrete Elements Subjected to Shear. *ACI Journal Proceedings* **83**(2).

Vermeer, P. A., De Borst, R. 1984. *Non-associated plasticity for soils, concrete and rock*, Heron, Delft, Netherlands.

Yeganeh, A. 2013. *Structural Behaviour Of Reinforced High Performance Concrete Frames Subjected To Monotonic Lateral Loading*, Master's thesis, Ryerson University, Toronto, Canada.

Wang, S., Li, V. 2004. Tailoring of Pre-existing Flaws in ECC Matrix for Saturated Strain Hardening *Proceedings of FRAMCOS*, Vail, Colorado, USA, **5**: 1005-1012.